Human Exposure to Field Radiated by Vertical Dipole Antenna over a Lossy Half-Space using Analytical Approach

Enida Cero Dinarević, *Fellow, IEEE*, Dragan Poljak, and Vicko Dorić

***Abstract*—The paper deals with an efficient procedure to study human exposure to vertical dipole antenna above a flat lossy half space. The closed form expressions for the corresponding irradiated electrical field are obtained assuming the sinusoidal and triangular current distribution along the antenna, respectively. The corresponding integral field expressions are evaluated by means of numerical integration and analytical procedures. The computations have been undertaken in the far field zone for various antenna parameters and compared to rigorous numerical model. Provided the field radiated from the vertical dipole is determined, whole body average Specific Absorption Rate (SAR_{WB}) is computed in a simple parallelepiped model of the human body and cylindrical model of the human body, respectively.**

***Index terms*—Human exposure, vertical dipole, radiated field, Specific Absorption Rate (SAR), parallelepiped model of the human body, cylindrical model of the human body.**

I. Introduction

One of the simplest scenarios to assess the human exposure to high frequency radiation is the human body exposed to the field radiated by thin wire antennas. Even with the sophisticated new technologies coming along, a simple body model exposed to dipole antenna radiation [1, 2] is of interest for quick dosimetry procedures, aiming to get a rapid estimation of the phenomena.

Thin wire radiation above a lossy half space was originally introduced by Sommerfeld in 1908 [3] and has been the subject of interest of many researches [3-9], mainly because of many applications, such as wireless telecommunications [7, 10], bioelectromagnetic, or surface wave propagation [11]. Moreover, small and directional antennas are used in 5G networks [12].

Calculation of electric field radiated by vertical dipole antenna requires the knowledge of the current distribution along the wire. The current distribution along the wire is governed by electric field integral equation (EFIE) for thin wires, also known as the Pocklington's integro-differential equation. The impact of lower lossy half space is taken into account via rigorous Sommerfeld integrals appearing within the integral equation kernel. Handling these integrals is rather tedious task and rather demanding in analytical or numerical sense (e.g. [11, 13]). Therefore, an approximate approach based on reflection coefficient approximation is very attractive in many engineering applications [11, 13, 14].

Traditional solution of the classical Sommerfeld problem uses Hertz potentials, but several difficulties may arise, such as problem with poor convergence and accuracy, or even with the appearance of spurious solutions [15]. Generally, as Sommerfeld-type integrals are highly oscillatory [3], difficult to evaluate numerically [3] and require intensive computational resources [16]. This complexity leads to development of numerous approximations, but the only feasible approach for obtaining a reliable, straightforward solution has been to integrate the Sommerfeld integrals numerically e.g. [14, 17].

Furthermore, numerical solution of Pocklington equation is demanding per se in a sense of accuracy, convergence and kernel quasi-singularity [11,13]. Therefore, some analytical simplifications under certain conditions are always welcome.

As a metric for exposure compliance determination, at frequency below 6 GHZ, according to Federal Communications Commission (FCC) and below 10 GHz, according to International Commission on Non-Ionizing Radiation Protection (ICNIRP), specific absorption rate (SAR) is used [18]. For upper limits calculation of Electromagnetic (EM) radiation effects numerical methods, such as the finite integration technique (FIT), for a complex heterogeneous model such as a voxel model of a human body, can be used [19]. Using voxels requires a high-performance hardware and software and limits calculation to one particular human body [19]. Since SAR is difficult to determine, electric field strength, which can be easily measured, can be used for SAR calculation [19]. Our paper proposes simple analytical method for SAR calculation using simplified parallelepiped geometry. Compared with approximate numerical approach and rigorous numerical approach, our analytical approach offers simplicity and saves computational resources. Model describes a complete analytical procedure for incident field and internal dosimetry using parallelepiped and cylindrical models of the human body. Model is good candidate for dosimetry of human exposure to radiation from 5G communication systems in lower portion of GHz frequency range.

This paper proposes closed form expressions for the corresponding irradiated electrical field assuming the

Manuscript received November 8, 2023; revised December 22, 2023. Date of publication January 30, 2024. Date of current version January 30, 2024. The associate editor prof. Giovanna Calò has been coordinating the review of this manuscript and approved it for publication.

Authors are with University of Split, Faculty of Electrical Engineering Mechanical Engineering and Naval Architecture, Split, Croatia (e-mails: enida.cero90@gmail.com, {dpoljak, vdoric}@fesb.hr).

Digital Object Identifier (DOI): 10.24138/jcomss-2023-0154

sinusoidal and triangular current distribution along the wire antenna. Irradiated electrical field is determined by means of numerical integration and analytical procedures. Provided the field radiated from the vertical dipole is determined, whole body averaged SAR, (SAR_{WB}) is computed in a simple parallelepiped model of the human body and compared to SAR_{WB} computed in a cylindrical model of the human body. Approximation which enables analytical solution of the field integrals as well as numerical approach uses Fresnel Reflection Coefficients Method (RCM). The use of RCM is related to the first term in the asymptotic expansion of the Sommerfeld integrals, which saves considerable computational time [5].

The paper is organized as follows: Section II outlines the integral representation of the electric field. Section III describes the assumed current distribution, while the electric field expressions are discussed in Section IV. Some computational examples are presented in Section V. Section VI describes electromagnetic dosimetry for both models. Finally, in section VII some general conclusions are given.

II. Problem Geometry

The geometry of the vertical dipole antenna with the human body model is shown in Fig. 1.

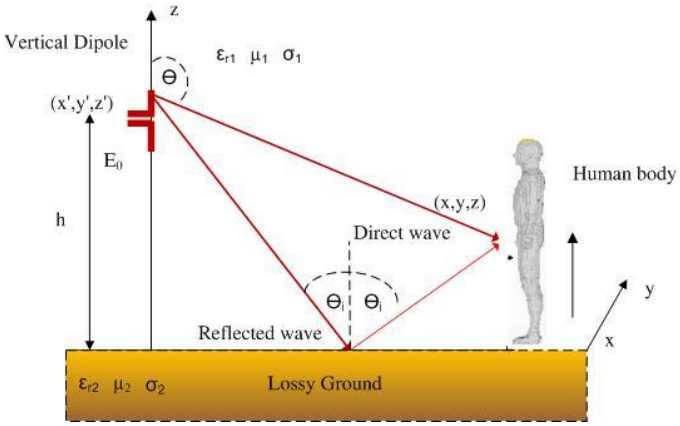

Fig. 1. Vertical dipole antenna above the lossy half space with human body model.

Antenna of length *L* is directed towards the positive z-axis at a certain height *h* above a lossy ground. Lower medium is dry, sandy and costal ground ($\mu = \mu_0, \varepsilon_r, \varepsilon_0, \sigma$), while the upper half space is free space (μ_0, ε_0). The dipole radiates time-harmonic electromagnetic waves at angular frequency $\omega = 2\pi f$ ($e^{-i\omega t}$ time dependence is assumed). Human body are located at (*x*, *y*, *z*) position, in horizontal plane.

Radius of vertical dipole antenna is negligible, i.e. much less than wavelength and the length of antenna (thin wire approximation – TWA [11,13]. The wire is assumed to be perfectly conducting (PEC). According to the TWA current is assumed to flow along the wire axis in *z* direction and vanishes at wire free ends.

Parameters of the antenna are strongly dependent on of the current distribution which is obtained as a solution of the Pocklington integro-differential equation in the frequency domain [20]:

$$E_z^{inc} = \frac{j}{\omega 4\pi\varepsilon_0}\left[\frac{\partial^2}{\partial z^2} + k_0^2\right]\int_{h-\frac{L}{2}}^{h+\frac{L}{2}} I(z')g(z,z')dz' \quad (1)$$

where E_z^{inc} stands for the incident field due to the voltage source and k_0 is free space wave number:

$$k_0 = \omega\sqrt{\mu_0\varepsilon_0} \quad (2)$$

Integral equation kernel is given by:

$$g(z,z') = g_0(z,z') + R_{TM}g_i(z,z') \quad (3)$$

where $g_0(z,z')$ is the free space Green function:

$$g_0(z,z') = \frac{e^{-jk_0R_0}}{R_0} \quad (4)$$

and $g_i(z,z')$ arises from the image theory:

$$g_i(z,z') = \frac{e^{-jk_0R_i}}{R_i} \quad (5)$$

R_0 and R_i denote the distance from the source and image antenna to the observation point:

$$R_0 = \sqrt{x^2 + y^2 + (z-z')^2} \quad (6)$$

$$R_i = \sqrt{x^2 + y^2 + (z+z')^2} \quad (7)$$

Furthermore, the reflecting properties of the lower medium have been taken into account via Fresnel [9-11, 13, 15] reflection coefficient for the transverse magnetic polarization:

$$R_{TM}^F = \frac{n\cos\theta - \sqrt{n - \sin^2\theta}}{n\cos\theta + \sqrt{n - \sin^2\theta}} \quad (8)$$

where the refraction index n and the angle of incidence θ are given by relations $n = \varepsilon_{eff}/\varepsilon_0 = \varepsilon_r - j\frac{\sigma}{\omega\varepsilon_0}$, $\theta = acot\frac{z+z'}{x}$ for numerical approach, and for analytical approach $\theta = acot\frac{h-z'}{x}$ and $\theta_i = acot\frac{h+z'}{x}$.

Here ε_r is the relative complex permittivity of the ground and σ is the ground conductivity.

In case of one single vertical antenna reflection coefficient is geometry independent (since $\theta = acot\frac{z+z'}{x}$ is then zero) and is given by its normal incidence form [21].

Generally, the Pocklington integro-differential equation (1) is numerically solved and the current distribution is obtained. When the current distribution along the wire is known or assumed the radiated field can be evaluated from the integral expression

$$E_z^{sct} = \frac{j}{\omega 4\pi\varepsilon_0}\left[\frac{\partial^2}{\partial z^2} + k_0^2\right]\int_{h-\frac{L}{2}}^{h+\frac{L}{2}} I(z')g(z,z')dz' \quad (9)$$

where E_z^{sct} stands for the scattered electric field.

In this paper numerical solution of Pocklington integro-differential equation is avoided by assuming the current distribution along the wire. Scattered electric field could then

be obtained by solving integral (9) using known current distribution.

The first goal of this work is the comparison between numerical and analytical approaches for handling expression (9) assuming the triangular and sinusoidal current distribution, respectively. It is convenient to use Fresnel approach for analytical solution, as well as for numerical solution, as already emphasized. Those solution are compared to rigorous numerical approach described in [22] and obtained using Numerical Electromagnetic Code (NEC) software. The second goal of this work is comparison between SAR_{WB} induced in parallelepiped and cylindrical human body model. In both cases the induced electrical field, and SAR, is a result of field irradiated by aforementioned vertical dipole antenna.

III. Radiated Field

The assumption of current distribution is the simplest way to determine the current distribution along vertical dipole antenna. Our previous work showed that numerical model with assumed current distribution (sinusoidal or triangular) gives satisfactory results for electrically small antennas [22] by decreasing the computational cost without appreciable loss of accuracy. The results of numerical approach with assumed current distribution are compared to rigorous numerical approach obtained from NEC. In rigorous numerical approach EFIE is solved by Method of Moments and the representation of current amplitudes over each wire segment exhibits the expected sinusoidal current distribution on wire. The assumed sinusoidal distribution is of the form:

$$I(z') = \frac{\sin\left(k\left(\frac{L}{2}-|z'-h|\right)\right)}{\sin\left(k\frac{L}{2}\right)} \tag{10}$$

while, for electrically shorter wire, i.e. for small argument of sinusoidal function, triangular distribution can be used:

$$I(z') = \frac{2I_0}{L}\left(\frac{L}{2} - |(z'-h)|\right) \tag{11}$$

where I_0 is the current maximum value, z' is the coordinate along the antenna and h is the height of the antenna above the half space.

Note that influence of the half space to current distribution waveform is assumed to be negligible since antenna is placed relatively high above the ground.

A. Numerical Approach

Based on assumed sinusoidal and triangular current distribution (10) and (11), respectively, the corresponding integral expressions for the tangential field are given by:

$$E_z^{sct} = \frac{1}{j\omega 4\pi\varepsilon_0}\left[\frac{\partial^2}{\partial z^2} + k_0^2\right]\int_{h-\frac{L}{2}}^{h+\frac{L}{2}} \frac{\sin\left(k\left(\frac{L}{2}-|z'-h|\right)\right)}{\sin\left(k\frac{L}{2}\right)} g(z,z')dz' \tag{12}$$

$$E_z^{sct} = \frac{1}{j\omega 4\pi\varepsilon_0}\left[\frac{\partial^2}{\partial z^2} + k_0^2\right]\int_{h-\frac{L}{2}}^{h+\frac{L}{2}} \frac{2I_0}{L}\left(\frac{L}{2} - |(z'-h)|\right) g(z,z')dz' \tag{13}$$

Expressions (12) and (13) are evaluated via adaptive numerical integration using Simpson formula.

B. Analytical Approach

The expression for the electric field in the case of sinusoidal (12) and triangular (13) current distribution are analytically solved using Fresnel approximation.

The amplitude of the total electric field is:

$$E_z^{tot} = E_z^{sctD} + E_z^{sctR} = E_z^{sctD} + R_{TM}E_z^{sctD} \tag{14}$$

where E_z^{sctD} is the amplitude of direct electric field in observation point, E_z^{sctR} is the amplitude of reflected electric field in observation point.

Using far field approximation and basic Fresnel approximation principles, after solving sample integrals the analytical solution of (14) could be obtained. Some mathematical details on the procedure are outlined in Appendix.

IV. Computational Examples

Parameters used for electric field calculation for both approaches is given in Table 1. According to the 5G Spectrum published by the Global System Mobile Alliance (GSMA) in March 2021, the 5G spectrum covers the millimeter wave range (24 GHz - 40 GHz), the medium range (3.3 - 4.2 GHz) and low frequency range (below 1 GHz). In the area of medium frequencies, coverage and capacity gain are best balanced, so this is the reason for a more detailed analysis of 5G systems at these frequencies in this paper. In addition, many systems operate in this frequency spectrum (3G/4G, Global Positioning System (GPS), Wireless Fidelity (Wi-Fi), L-band satellite communication, S-band C-band radars), which further implies that a large number of small cells must be implemented to reduce interference at each base station, with the antennas small and directional [23].

TABLE I
THE VALUES OF USED PARAMETERS

Parameter	*Value*
Frequency [GHz]	3
Length of antenna [m]	0.01
Height above the ground [m]	20
Ground relative permittivity	10
Ground conductivity [mS/m]	1
I_0 [A]	1

The length of the antenna is chosen so that the antenna is considered electrically small, and that the maximum current is normalized to 1. Other parameters are chosen in accordance with the characteristics of the environment in which the antenna is located.

A. The Influence of Antenna Height above Ground on Radiated Electric Field

Depending on the application, the height of the antenna above the ground varies. Changing the height of the antenna above the ground plane leads to the well-known lobbing effect

[24], in such a way that the number of lobes increases with increase of height.

The radiated electric field is calculated in the upper medium in a fixed horizontal direction (x=200 m, y=0 m) away from the antenna (which corresponds to a far field zone), while in the vertical direction z changes from 0 m to 1.8 m above ground. Following antenna heights are of interest: 10 m and 20 m.

The absolute value of the electric field radiated in the air versus point location in the z axis for a fixed distance from the source in an x horizontal direction x = 200 m and at an antenna height of 10 m above are shown in Fig. 2 (a) and Fig. 2 (b), and 20 m in Fig. 3 (a) and Fig. 3 (b). The electric field values are compared to values obtained from NEC. Fig. 2 (a), Fig. 2 (b), Fig 3 (a), and Fig. 3 (b), contain curves obtained via numerical and analytical approach with sinusoidal and triangular current distribution and obtained via rigorous numerical approach.

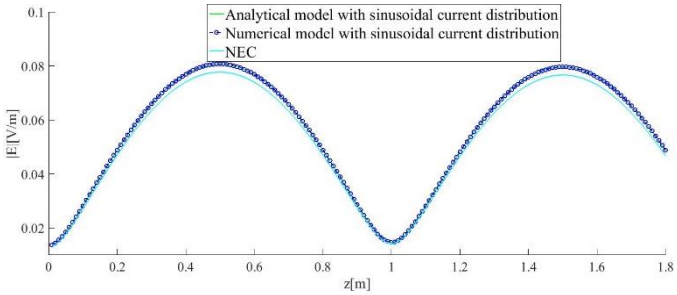

Fig. 2. (a) The absolute value of the electric field radiated in the air versus point location in the *z* axis for a fixed distance from the source in an *x* horizontal direction *x* = 200 m, frequency f = 3 GHZ, and at an antenna height of 10 m above ground and sinusoidal current distribution.

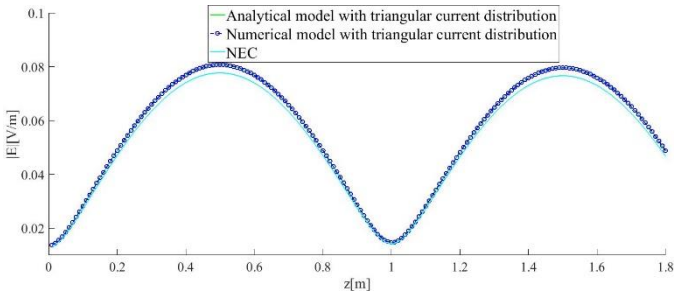

Fig. 2. (b) The absolute value of the electric field radiated in the air versus point location in the z axis for a fixed distance from the source in an x horizontal direction x = 200 m, frequency f = 3 GHZ, and at an antenna height of 10 m above ground and triangular current distribution.

Previously mentioned lobbying effect is clearly noticeable from Fig. 2 - Fig. 3. Based on the Fig. 2 and Fig. 3 the maximum value of the radiated electric field is the same for numerical and analytical approach and for heights of 10 m and 20 m above the ground. Maximal values are higher for analytical and numerical approach when compared to rigorous numerical model, Fig. 2 (a), Fig. 2 (b), Fig. 3 (a), and Fig. 3 (b).

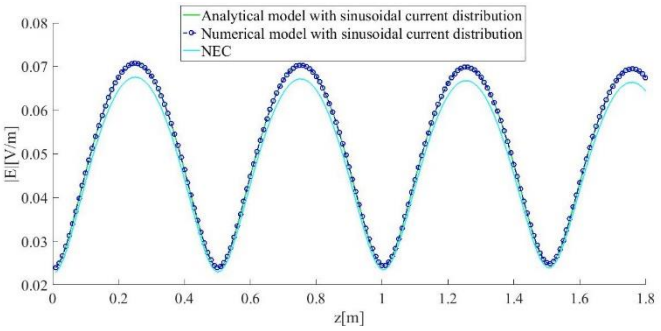

Fig. 3. (a) The absolute value of the electric field radiated in the air versus point location in the z axis for a fixed distance from the source in an x horizontal direction x = 200 m, frequency f = 3 GHZ, and at an antenna height of 20 m above ground and sinusoidal current distribution.

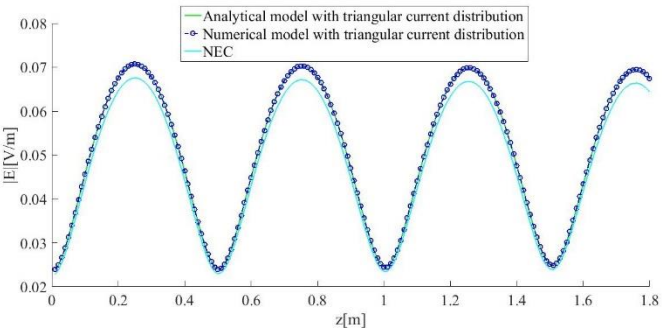

Fig. 3. (b) The absolute value of the electric field radiated in the air versus point location in the z axis for a fixed distance from the source in an x horizontal direction x = 200 m, frequency f = 3 GHZ, and at an antenna height of 20 m above ground and triangular current distribution.

With antenna elevation the difference between electric field values for analytical and numerical approach with assumed current distribution compared to rigorous numerical approach increases, being maximal at curves maximums.

There is no difference in electric field values that arise under the assumption of sinusoidal or triangular current distribution on the antenna. In other words, absolute difference between absolute electric field values radiated in the air by analytical and numerical approach versus point location in the z axis for a fixed distance from the source in an x horizontal direction x = 200 m totally agree. The electric field waveforms for the analytical and numerical approach are the same, with the largest difference compared to rigorous numerical approach being noticeable in the region of the maximum.

At height of 10 m and 20 m respectively above the ground, the maximum absolute difference between field radiated in the air by analytical and approximate numerical approach compared to rigorous numerical approach is less than 1 %. Thus, the models based on approximate approach agree satisfactorily with the rigorous numerical model.

In conclusion, when the height of the antenna above the ground is less than 200*wavelength the results obtained via the approximate analytical and numerical approach agree satisfactorily.

B. The Influence of the Electrical Length of the Antenna on Radiated Electric Field

The second example provides the absolute value of the electric field when $\frac{L}{\lambda}$ changes during the calculation. Three ratios observed are: $\frac{L}{\lambda}=\frac{1}{10}$, $\frac{L}{\lambda}=\frac{1}{4}$ and $\frac{L}{\lambda}=\frac{1}{2}$. The impact of $\frac{L}{\lambda}$ on electrical field is shown in Fig. 3 (a), Fig. 3 (b), Fig. 4 (a), Fig. 4 (b), Fig. 5 (a), and Fig. 5 (b). The absolute value of the electric field radiated in the air versus point location in the z axis for a fixed distance from the source in an x horizontal direction x = 200 m and of $\frac{L}{\lambda}=\frac{1}{10}$ is shown in Fig. 3 (a) and Fig. 3 (b), $\frac{L}{\lambda}=\frac{1}{4}$ in Fig. 4 (a) and Fig 4 (b), and $\frac{L}{\lambda}=\frac{1}{2}$ in Fig. 5 (a) and Fig 5 (b).

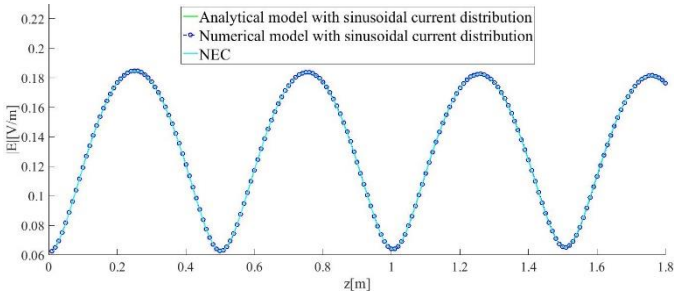

Fig. 4. (a) The absolute value of the electric field radiated in the air versus point location in the z axis for a fixed distance from the source in an x horizontal direction x = 200 m, frequency f = 3 GHZ, and of $\frac{L}{\lambda}=\frac{1}{4}$ and sinusoidal current distribution.

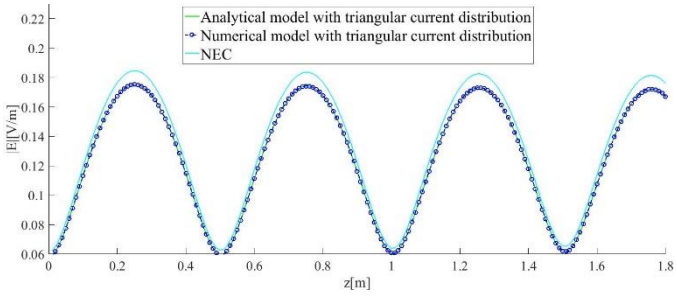

Fig. 4. (b) The absolute value of the electric field radiated in the air versus point location in the z axis for a fixed distance from the source in an x horizontal direction x = 200 m, frequency f = 3 GHZ, and of $\frac{L}{\lambda}=\frac{1}{4}$ and triangular current distribution.

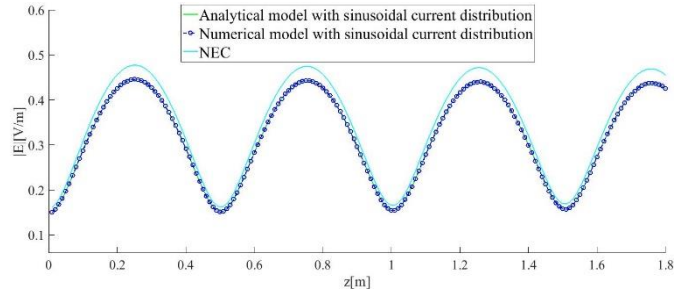

Fig. 5. (a) The absolute value of the electric field radiated in the air versus point location in the z axis for a fixed distance from the source in an x horizontal direction x = 200 m, frequency f = 3 GHZ, and of $\frac{L}{\lambda}=\frac{1}{2}$ and sinusoidal current distribution.

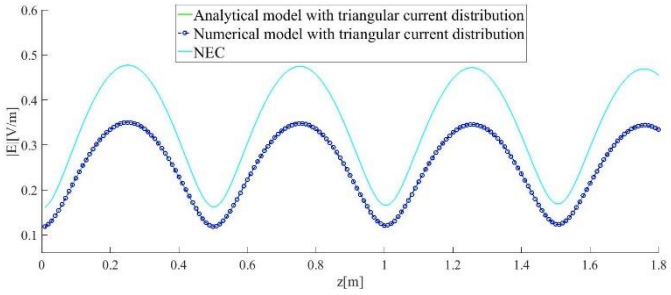

Fig. 5. (b) The absolute value of the electric field radiated in the air versus point location in the z axis for a fixed distance from the source in an x horizontal direction x = 200 m, frequency f = 3 GHZ, and of $\frac{L}{\lambda}=\frac{1}{2}$ and sinusoidal triangular distribution.

Figs. 3 - 5 clearly show that the field increases as the ratio of physical length and wavelength increase. In other words, physically large antennas generate a larger electric field. The maximum value increases from 0.07 V/m to 0.45 V/m when $\frac{L}{\lambda}$ increases from $\frac{1}{10}$ to $\frac{1}{2}$ for analytical and numerical model with sinusoidal current distribution, and from 0.07 V/m to 0.35 V/m when the $\frac{L}{\lambda}$ increases from $\frac{1}{10}$ to $\frac{1}{2}$ for analytical and numerical model with triangular current distribution. The maximum value increases from 0.065 V/m to 0.47 V/m when the $\frac{L}{\lambda}$ increases from $\frac{1}{10}$ to $\frac{1}{2}$ for rigorous numerical approach.

As $\frac{L}{\lambda}$ increases, the difference between electric field also increases for sinusoidal and triangular current distribution (Fig. 3 – Fig. 5). It should be noted that in all cases the largest difference between field values is observed at the peaks and it is larger for approximate models with triangular current distribution compared to sinusoidal current distribution.

The maximum absolute difference between absolute electric field values radiated in the air by approximate numerical approach and analytical approach with assumed current distribution is less than 2 % compared to rigorous numerical approach for $\frac{L}{\lambda}=\frac{1}{10}$.

For electrically middle-sized antennas the maximum absolute difference between absolute electric field values radiated in the air by numerical and analytical approach with assumed triangular current distribution is less than 5 % for $\frac{L}{\lambda}=\frac{1}{4}$.

Further on, the maximum absolute difference between absolute electric field values radiated in the air by rigorous numerical approach with assumed sinusoidal current distribution is less than 5 % for $\frac{L}{\lambda}=\frac{1}{2}$, and with assumed triangular current distribution is less than 15 % for $\frac{L}{\lambda}=\frac{1}{2}$.

Consequently, for electrically larger antennas the appriximation with triangular current distribution should be avoided and more accurate results can be obtained by using the sinusoidal current distribution.

This leads to the conclusion that for electrically small antennas ($\frac{L}{\lambda}\leq\frac{1}{10}$) approximate analytical and numerical approach, respectively provides satisfactory results for sinusoidal and triangular current distribution.

C. Radiated Electric Field distribution along the x axes

Fig. 6, Fig. 7, Fig. 8, and Fig. 9 clearly show that the field decreases as the distance from the source increases (from 20 m to 200 m).

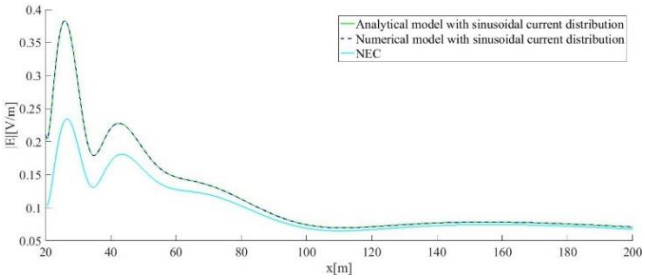

Fig. 6. The absolute value of the electric field radiated in the air versus point location in the x axis for a fixed distance in an z vertical direction z = 0.25 m, frequency f = 3 GHZ, and at an antenna height of 20 m above ground and sinusoidal current distribution.

The maximum value of electric field is 0.46 V/m (for approximate numerical and analytical model) and 0.23 V/m (for rigorous numerical approach) and it is obtained at point (20 m, 0 m, 1.75 m). The field amplitude approaches the same value as *x* increases for both models. In all analyzed scenarios, the absolute value of the electric field radiated in the air drops below 0.2 V/m when the distance in the horizontal direction increases to 40 m. When the distance in the horizontal direction is above 60 m these three models agree satisfactorily.

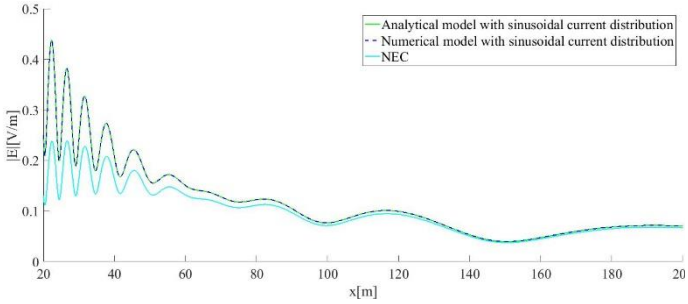

Fig. 7. The absolute value of the electric field radiated in the air versus point location in the x axis for a fixed distance in an z vertical direction z = 0.75 m, frequency f = 3 GHZ, and at an antenna height of 20 m above ground and sinusoidal current distribution.

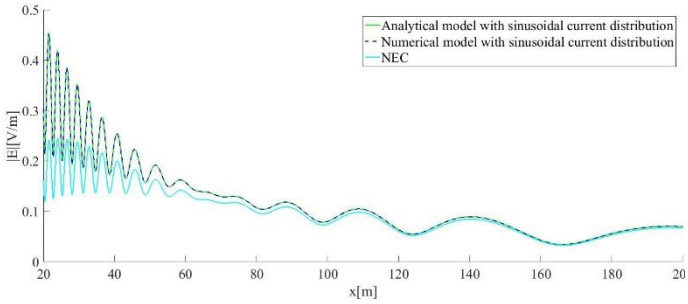

Fig. 8. The absolute value of the electric field radiated in the air versus point location in the x axis for a fixed distance in an z vertical direction z = 1.25 m, frequency f = 3 GHZ, and at an antenna height of 20 m above ground and sinusoidal current distribution.

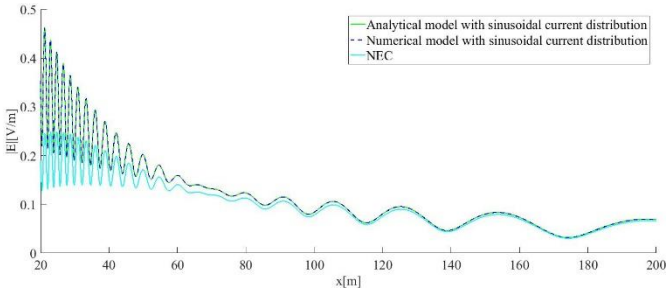

Fig. 9. The absolute value of the electric field radiated in the air versus point location in the x axis for a fixed distance in an z vertical direction z = 1.75 m, , frequency f = 3 GHZ, and at an antenna height of 20 m above ground and sinusoidal current distribution.

For small distances in the horizontal direction (x < 40 m), due to the far field approximation used in proposed model, the significant overestimation of the field values could be observed. The results of rigorous numerical approach obtained from NEC consider the formulations for EMF in near field, meaning that they include the terms 1/R^2and 1/R^3. Our analytical solution is based on far field approximation, and takes only field dependence of term 1/R, which is his main limitation.

The absolute value of the electric field radiated in the free space versus point location for z = 1.75 m and sinusoidal current distribution is shown in Fig. 10.

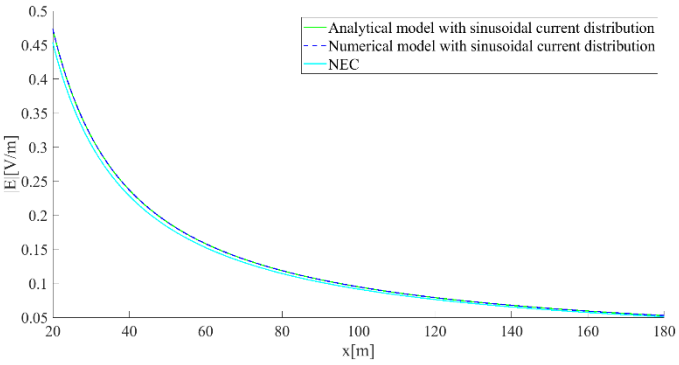

Fig. 10. The absolute value of the electric field radiated in the free space versus point location in the x axis for a fixed distance in an z vertical direction z = 1.75 m, frequency f = 3 GHZ, and sinusoidal current distribution.

There are no differences between electric field values radiated in free space by the approximate numerical approach and the analytical approach with assumed current distribution. And the difference between the mentioned approaches is very small compared to the rigorous numerical approach. In other words, the results of our analytical approach almost completely agree with the results of approximate numerical approach with assumed current distribution and the results of rigorous numerical approach in free space.

Comparing results between the rigorous formulation and far field approximation in the case of the free space and a lossy media clearly demonstrates that the presence of the lossy ground somehow expands the near field region thus reducing the accuracy of proposed procedure.

V. Assessment of SAR in the Simplified Body Models

Two representations of the human body are considered in this part of the work: simple parallelepiped model of the human body and cylindrical human body model. The human body is exposed to incident field in chapters III and IV. EM dosimetry in parallelepiped human body model is considered as mathematically simpler compared to cylindrical human body model. The small differences in calculated whole body average SAR imply that the proposed approaches are useful in getting rapid estimation of the phenomenon in average sense, without significant loss of accuracy. This chapter aims to compare the values of whole body average SAR for two different models.

A. SAR in Parallelepiped Human Body Model

Quantification of the effects of electromagnetic radiation on the human body is performed by SAR, Power Density (PD), or internal fields, depending on operational frequency [25- 27]. According to ICNIRP for frequencies below 6 GHz and above 100 kHz, SAR should be used, for frequencies above 6 GHz PD should be used, and bellow 100 kHz Internal electric field should be used [23]. SAR (W/kg) at any point in the human skin is proportional to internal electric field [28]:

$$SAR_0 = \frac{\sigma}{2\rho}|\Gamma_{tr}|^2|E_0|^2 \tag{15}$$

$$\Gamma_{tr}^{MIT} = \frac{2n}{n+1} \tag{16}$$

where σ and ρ are electric conductivity and density of the biological tissue, respectively (in this case human skin), and E_0 is the peak value of the field at the surface of the parallelepiped and the transmission coefficient arising from the modified image theory (MIT) [15, 29, 30, 31, 32]. Conductivity may significantly vary in different tissues, and increases considerably and non-linearly with frequency. The average conductivity of the human skin is assumed to be 0.1 S/m [33]. Skin density is constant on all frequencies, and the used value is 1010 kg/m^3.

Fig. 11 shows the parallelepiped human body model with height of H, depth of D, and width of W placed at position (x, 0, 0) and exposed to radiation of vertical dipole antenna at height h above the ground.

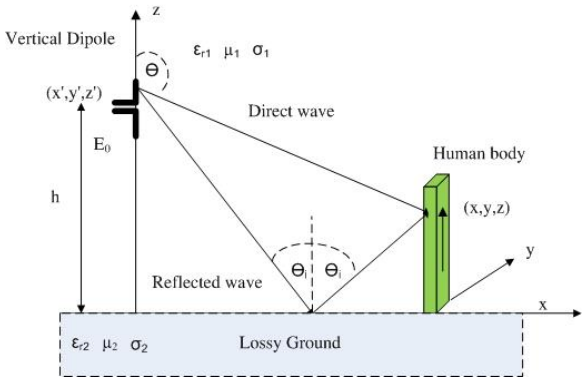

Fig. 11. Parallelepiped human body model, dimensions: 180 cm(H), 40 cm (D), 20 cm (W)

SAR averaged over a whole bode is given by [34]:

$$SAR_{WB} = \frac{1}{V}\int_V SAR_{surf}\,dV \tag{17}$$

where SAR_{surf} is assumed to decrease exponentially through the body, as follows [35]

$$SAR_{surf} = SAR_0 e^{-\frac{2x}{\delta}} \tag{18}$$

and skin depth is given by:

$$\delta = \sqrt{\frac{2}{\omega\mu\sigma}} \tag{19}$$

Inserting (19) in (20) leads to:

$$SAR_{WB} = \frac{1}{V}\int_V SAR_0 e^{-\frac{2x}{\delta}}dV = \frac{\delta}{2\Delta x}SAR_0\left(1 - e^{-\frac{2\Delta x}{\delta}}\right) \tag{20}$$

B. SAR in Cylindrical Human Body Model

The human body is represented by a cylinder, whose length L = 1.8 m corresponds to the height of the body, and radius a = 20 cm, and assumed to be vertically positioned on PEC and exposed to High Frequency (HF) field (Fig. 12). The average value of the conductivity of the human skin is assumed to be 0.1 S/m.

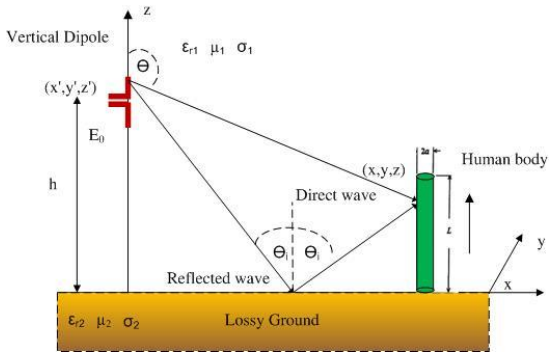

Fig. 12. Cylindrical human body model, radius: 20 cm

Axial current induced in the body is governed by the Pocklington integrodifferential equation, derived from the continuity condition for the tangential electric field components [36]:

$$E_z^{inc} + E_z^{sct} = I(z)Z_c(z) \tag{21}$$

where $I(z)$ is induced axial current, and $Z_L(z)$ is the impedance per unit length of the finitely conductive cylinder.

Starting from Maxwell equations and performing some mathematical manipulation, Pocklington's integro-differential equation for imperfectly conducting thick wire is obtained [37]:

$$E_z^{inc} = \frac{1}{j4\pi\omega\varepsilon_0}\int_{-L_c}^{L_c}\left(\frac{\partial^2}{\partial z^2} + k^2\right)g_E(z,z')I(z')dz' + I(z)Z_c(z) \tag{22}$$

where $g_E(z,z')$ is the so-called exact Green function for the thick cylinder given by

$$g_E(z,z') = \frac{1}{2\pi}\int_0^{2\pi}\frac{1}{R}d\varphi \tag{23}$$

where:

$$R = \sqrt{(z-z')^2 + \left(2a\sin\frac{\varphi}{2}\right)^2} \tag{24}$$

In the HF region, the impedance per unit length is given by [37]:

$$Z_c(\zeta) = \frac{1}{a^2\pi\sigma}\left(\frac{ka}{2}\right)\frac{J_0(j^{-1/2}k\zeta)}{J_1(j^{-1/2}ka)} + Z_c \tag{25}$$

The current density induced in the body can be expressed in terms of the axial current I_c as follows [35, 37]:

$$J_z(\zeta,z) = \frac{I_c(z)}{a^2\pi}\left(\frac{ka}{2}\right)\frac{J_0(j^{-1/2}k\zeta)}{J_1(j^{-1/2}ka)} \tag{26}$$

where ζ ranges from 0 to a, z is the radius of cylinder, J_0 and J_1 are the Bessel functions, and k is the free space phase constant.

The induced electric field at any point $T(\zeta,z)$ inside cylindrical model of the body is given by [37]:

$$E_z(\zeta,z) \approx \frac{J_z(\zeta,z)}{\sigma+j\omega\varepsilon} \tag{27}$$

The whole body averaged SAR is given by (17).

VI. Computation Results

Figs. 13-16 show the SAR_{WB} versus point location in the x axis for a fixed distance in an z vertical direction corresponding to field maximus z = 0.25 m, z = 0.75 m, z = 1.25 m, and z = 1.75 m, frequency of 3 GHz and at antenna height of 20 m above ground. SAR_{WB} is calculated using previously obtained values of incident electric field.

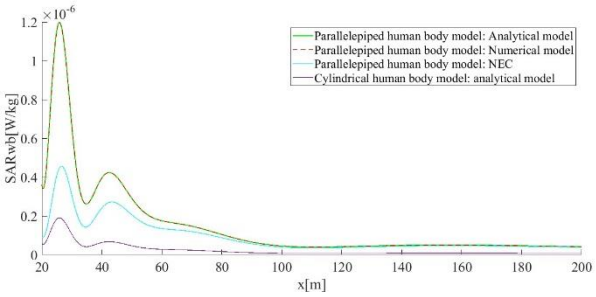

Fig. 13. SAR averaged over a whole bode versus point location in the x axis for a fixed distance from the source in an z vertical direction z= 0.25 m, frequency f = 3 GHZ and h =20m and sinusoidal current distribution.

Spatial distributions for the SARWB are following the same pattern as the corresponding electric field distributions as expected. According to the [38], the maximum value of SAR averaged over whole body should not exceed 0.4 W/kg for workers and 0.08 W/kg for the general public. According to Fig. 14, Fig. 15, Fig. 16, and Fig. 17 whole-body average SAR is bellow limits defined by ICNIRP in all analyzed cases.

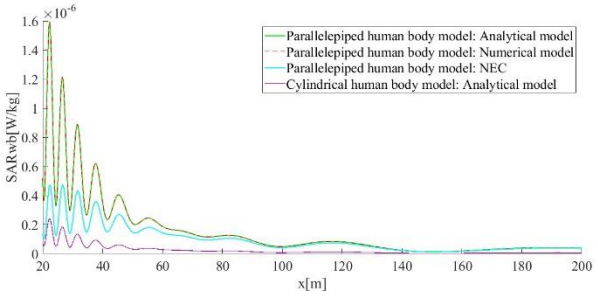

Fig. 14. SAR averaged over a whole bode versus point location in the x axis for a fixed distance from the source in an z vertical direction z= 0.75 m, frequency f = 3 GHZ and h =20m and sinusoidal current distribution.

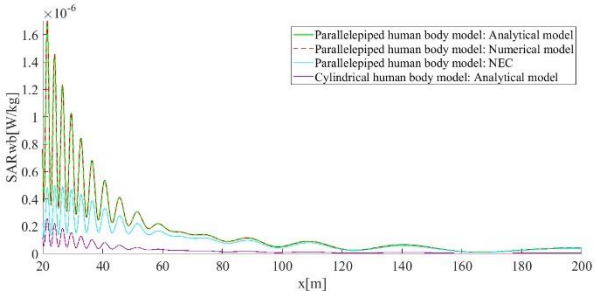

Fig. 15. SAR averaged over a whole bode versus point location in the x axis for a fixed distance from the source in an z vertical direction z= 1.25 m, frequency f = 3 GHZ and h =20m and sinusoidal current distribution.

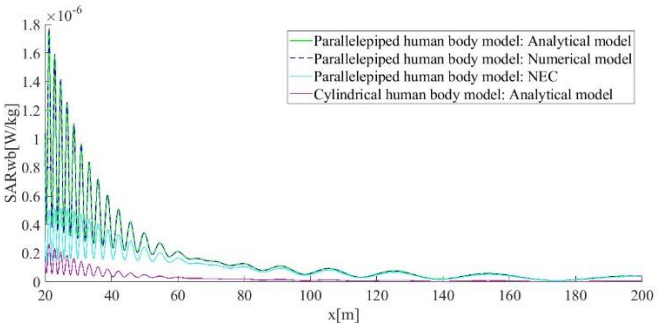

Fig. 16. SAR averaged over a whole bode versus point location in the x axis for a fixed distance from the source in an z vertical direction z= 1.75 m, frequency f = 3 GHZ and h =20m and sinusoidal current distribution.

Maximum value of whole body averaged SAR is obtained using the approximate analytical and numerical models in parallelepiped human body model and it is obtained at point around 26 m from source in x direction, and is less than $1.2 \cdot 10^{-6}\,W/kg$. In case of NEC model, the maximum is less than $0.46 \cdot 10^{-6}\,W/kg$, and in cylindrical human body model the maximum of whole body averaged SAR obtained in this point is less than $0.2 \cdot 10^{-6}\,W/kg$.

This difference between whole body averaged SAR obtained using analytical models, in parallelepiped and cylindrical human body models,-falls below 10 % at 80 m and reaches the value less than 1 % at 200 m from source antenna in x horizontal direction. Generally, positioning of human body model far away from source antenna enables simpler human body modeling. Therefore, the simplified models may help to provide a good knowledge of the EM behavior of parallelepiped and

cylindrical living tissues in far field zone.

VII. Conclusion

The paper deals with an efficient procedure to study human exposure to vertical dipole antenna above a flat lossy half space. The results obtained using closed form expressions for the irradiated electrical field with assumed sinusoidal and triangular current distribution agree satisfactorily with numerical approach when the height of the antenna above the ground is $h < 200 * \lambda$. Further on, analytical and numerical approach, provides satisfactory results for sinusoidal and triangular current distribution for electrically small antennas ($L/\lambda \leq 1/10$). For electrically larger antennas ($L/\lambda = 1/4$) the approximation with triangular current distribution should be avoided and more accurate results can be obtained by using the sinusoidal current distribution.

The absolute value of the electric field radiated in the air drops below $0.2\,V/m$ when the distance in the horizontal direction increases to 40 m, and three models agree satisfactorily when the distance in the horizontal direction is $x > 60\,m$.

SAR_{WB} computed in a simple parallelepiped and cylindrical models of the human body is bellow limits defined by ICNIRP in all analyzed cases. Maximum value of SAR_{WB} obtained for approximate analytical and numerical models in parallelepiped is less than $1.6\,x10^{-6}W/kg$).

Bearing in mind that the electric field and SAR values obtained by means of analytical approach are higher than the ones corresponding to the results obtained via more rigorous numerical modeling it can be concluded that such an overestimation is acceptable for the health risk assessment. Namely, if the overestimated values do not exceed exposure limits it is ensured that the values stemming from realistic scenarios from either computation or measurement will stay within the proposed limits.

Model exposed to dipole antenna radiation gives satisfactory results and could be used for quick dosimetry procedures, aiming to get a rapid estimation of the phenomena.

References

[1] K. Li et al., "Intercomparison of Calculated Incident Power Density and Temperature Rise for Exposure from Different Antennas at 10–90 GHz," in *IEEE Access*, vol. 9, pp. 151654-151666, 2021, doi: 10.1109/ACCESS.2021.3126738.

[2] D. Poljak, V. Dorić and A. Šušnjara, "Absorbed Power Density at the Surface of Planar Tissue due to Radiation of Dipole Antenna," *2021 6th International Conference on Smart and Sustainable Technologies (SpliTech)*, Bol and Split, Croatia, 2021, pp. 1-6, doi: 10.23919/SpliTech52315.2021.9566442.

[3] P. Parhami, R. Mittra, "Analysis of arbitrarily shaped wire antennas radiating over a lossy half-space," *IEEE Transactions on Antennas and Propagation*, Vol. 28, pp. 397-403, May 1980.

[4] D. Poljak, V. Doric, K. E. Khamlichi Drissi, M. Chaaban and C. Garrec, "Vertical dipole above a PEC ground representing a part of a PLC system — Numerical versus analytical study*"*, in *Proc. of 20th International Conference on Software, Telecommunications and Computer Networks*, 2012.

[5] A. Šarolić, D. Senić, Z. Živković, "Radiation Pattern of a Vertical Dipole over Sea and Setup for Measuring thereof*"*, *Journal for Control, Measurement, Electronics, Computing and Communications*, Vol. 53, pp. 5-58, 2012.

[6] A. Chrysostomou, S. Bourgiotis, S. Sautbekov, K. Ioanniand, i P.V. Frangos, "Radiation of a Vertical Dipole Antenna over Flat and Lossy Ground: Accurate Electromagnetic Field Calculation using the Spectral Domain Approach along with Redefined Integral Representations and corresponding Novel Analytical Solution*"*, *Elektronika IR Electrotechnika*, Vol. 22, pp. 54–61, Feb. 2016.

[7] S. Bourgiotis, A. Chrysostomou, K. Ioannidi, S. Sautbekov, P. Frangos, "Radiation of a vertical dipole over flat and lossy ground using the spectral domain approach: comparison of stationary phase method analytical solution with numerical integration results*"*, *Elektronika ir Elektrotechnika*, Vol. 21, pp. 38–41, June 2015.

[8] K. A. Michalski, H.-I. Lin, "On the far-zone electromagnetic field of a vertical Hertzian dipole over an imperfectly conducting half-space with extensions to plasmonics*"*, *Radio Sci.*, Vol. 52, pp. 798–810, July 2017.

[9] S. Sautbekov, "Sommerfeld half-space problem revisited: Short-wave asymptotic solutions*"*, Preprint submitted to Elsevier, 2020.

[10] K. Ioannidi, C. Christakis, S. Sautbekov, P. Frangos, S.K. Atanov, "The radiation problem from a vertical Hertzian dipole antenna above flat and lossy ground: novel formulation in the spectral domain with closed-form analytical solution in the high frequency regime", *Int. Journal Antennas and Propagation (IJAP)*, Vol. 2014, Jan. 2014.

[11] D. Poljak, "Advanced Modeling in Computational Electromagnetic Compatibility*"*, *New Jersey: John Wiley & Sons*, Inc., 2007.

[12] T. Hong, S. Zhen, R. Liu, W. Zhao, "Design of mmWave Directional Antenna for Enhanced 5G Broadcasting Coverage", *Sensors (Basel)*, Vol. 21, No.3, pp. 746-765.

[13] D. Poljak, K. El Khamlichi Drissi, "Computational Methods in Electromagnetic Compatibility", *New Jersey: John Wiley & Sons*, Inc., 2018.

[14] G. J. Burke, E.K. Miller, J.N. Brittingham, D. L. Lager, R. J. Lytle and J. T. Okada, "Computer modeling of antennas near the ground", *Electromagnetics*, Vol. 1(1), pp. 29-49, Feb. 1981.

[15] A. Šušnjara, D. Poljak and V. Dorić, "Electric field radiated by a dipole antenna above a lossy half space: Comparison of plane wave approximation with the modified image theory approach", in *Proc. of 25th International Conference on Software, Telecommunications and Computer Networks (SoftCOM)*, 2017.

[16] M. Fernandez Pantoja, A.G. Yarovoy, A. Rubio Bretones, S. Gonzalez Garcia, "Time domain analysis of thin-wire antennas over lossy ground using the reflection-coefficient approximation", *Radio Science*, Vol. 44. Dec. 2009.

[17] S. Bourgiotis, P. Frangos, S. Sautbekov, M. Pshikov, "The Evaluation of an Asymptotic Solution to the Sommerfeld Radiation Problem Using an Efficient Method for the Calculation of Sommerfeld Integrals in the Spectral Domain", *Electronics*, Vol. 10, June 2021.

[18] T. Wu, T. S. Rappaport, C. M. Collins, "The Human Body and Millimeter-Wave Wireless Communication Systems: Interactions and Implications", In *Proc. Of IEEE International Conference on Communications (ICC)*, Jun. 2015.

[19] J. Grund, K.-U. Rathjen, C. Radel, M. Stiemer, S. Dickmann, "Planar Multilayer Model of Human Tissue Exposed to a Plane Electromagnetic Wave", *IEEE Journal od Electromagnetics, RF, and Microwave in Medicine and Biology*, Vol. 5, No. 4, pp. 305-403, Dec. 2021.

[20] D. Poljak, K. El Khamlich Drissi, K. Kerroum, S. Sesnic, "Comparison of analytical and boundary element modeling of electromagnetic field coupling to overhead and buried wires", *Engineering Analysis with Boundary Elements*, Vol. 35, pp. 666-563, Nov. 1977.

[21] E. K. Miller, A. J. Pioggio, G. J. Burke, E. S. Selden, "Analysis of Wire Antennas in the Presence of a Conducting Half-Space. Part II. The Horizontal Antenna in Free Space", *Canadian Journal of Physics*, Vol. 50, Nov. 1972.

[22] E. Cero Dinarević, D. Poljak, V. Dorić, "Electric Field Radiated By a Vertical Dipole Antenna Above a Lossy Half Space by using Calculated and Assumed Current Distribution", In *Proc. of 7th International Conference on Smart and Sustainable Technologies (SpliTech)*, July 23-26, 2022.

[23] D. H. Gultekin, P. H. Siegel, "Absorpition of 5G Radiation in Brain Tissue as a Function of Frequency, Power, and Time", *IEEE Access*, Vol. 8, pp. 115593 – 115612, 2020.

[24] Y. Huang, "An efficient analysis of vertical dipole antennas above a lossy half-space", Master of Science, Clemson University, 2007. Accessed on: March 29, 2022. [Online]. Available: https://tigerprints.clemson.edu/all_theses/147.

[25] A. Kanezaki, S. Watanabe, A. Hirata and H. Shirai, "Theoretical Analysis for Temperature Elevation of Human Body Due to Millimeter Wave

Exposure", In *Proc. of Cairo International Biomedical Engineering Conference*, 2008, pp. 1-4.
[26] D. Poljak, A. Šušnjara and L. Kraljević, "Absorbed Power Density in a Multilayer Tissue Model due to Radiation of Dipole Antenna at GHz Frequency Range: Part I Theoretical Background", In *Proc. of 7th International Conference on Smart and Sustainable Technologies (SpliTech)*, 2022, pp. 1-4.
[27] D. Poljak, A. Šušnjara and L. Kraljević, "Absorbed Power Density in a Multilayer Tissue Model due to Radiation of Dipole Antenna: Part II Results", In *Proc. of 7th International Conference on Smart and Sustainable Technologies (SpliTech)*, 2022, pp. 1-5.
[28] D. Poljak, M. Cvetković, et al., "Boundary integral methods in bioelectromagnetic and biomedical applications of electromagnetic fields", *WIT Transactions on Engineering Sciences*, Vol. 122, pp. 85-94, 2019.
[29] D. Poljak, et al., "Comparison of wire antenna and modified transmission line approach to the assessment of frequency response of horizontal grounding electrodes", *Engineering Analysis with Boundary Elements*, Vol. 32, pp. 676-681, March 2008.
[30] D. Poljak, N. Kovač, "Time domain modeling of a thin wire in a two-media configuration featuring a simplified reflection/ transmission coefficient approach", *Engineering Analysis with Boundary Elements*, Vol. 33, pp.283-293, July 2009.
[31] D. Poljak, S. Šesnić, D. Paric and K. El Khamlichi Drissi, "Direct time domain modeling of the transient field transmitted in a dielectric half-space for GPR applications", In *Proc. of International Conference on Electromagnetics in Advanced Applications (ICEAA)*, 2015, pp. 345-348.
[32] M. Galić, D. Poljak, V. Dorić, "Simple analytical models for the calculation of the electric field radiated by the base station antenna", *International Journal for Engineering Modelling*, Vol. 31, No. (1-2), pp. 31-42, 2018.
[33] A. Hirata, Y. Takano, Y. Kamimura, O. Fujiwara, "Effect of Averaging Volume and Algorithm on In-Situ Electric Field for Uniform Electric and Magnetic Field Exposures", *Physics in Medicine and Biology*, Vol. 55 (9), pp. 243-252, May 2010.
[34] International Commission on Non-Ionizing Radiation Protection, The new ICNIRP radiofrequency guidelines, December 2, 2019. Accessed on: May 11, 2020. [Online]. Available: https://www.itu.int/en/ITU-D/Regional-Presence/ArabStates/Documents/events/2019/EMF/ICNIRP%20RF%20guidelines%20ITU%20Amman%20Dec%202019.pdf.
[35] D. Poljak, C. Y. Tham, O. Gandhi and A. Sarolic, "Human equivalent antenna model for transient electromagnetic radiation exposure," in *IEEE Transactions on Electromagnetic Compatibility*, vol. 45, no. 1, pp. 141-145, Feb. 2003, doi: 10.1109/TEMC.2002.808042.
[36] D., Poljak, C.Y., Tham, O., Gandhi, et al., "The assessment of human exposure to low frequency and high frequency electromagnetic fields using the boundary element analysis", *Engineering Analysis with Boundary Elements*, Vol. 27, pp. 999–1007, 2003.
[37] D., Poljak, N., Kovač, "Simplified Electromagnetic-thermal Analysis of Human Exposure to Radiation from Base Station Antennas", *ATKAAF*, Vol. 45(1-2), pp. 11–17, 2004.
[38] ICNIRP: ICNIRP Guidelines for limiting exposure to electromagnetic fields (100 kHz to 300 GHz), *HEALTH PHYS*, Vol. 118, No. 5, pp. 483–524, 2020.

APPENDIX A

The scattered electric field is given by:

$$E_z^{sct} = \frac{1}{j\omega 4\pi\varepsilon_0}\frac{\partial^2}{\partial z^2}\int_{h-\frac{L}{2}}^{h+\frac{L}{2}} I(z')g(z,z')dz' + \frac{j}{\omega 4\pi\varepsilon_0}k_0^2\int_{h-\frac{L}{2}}^{h+\frac{L}{2}} I(z')g(z,z')dz' \quad (1)$$

The first addition in (1) is very small in the far field zone, so it can be neglected. Thus, expression for the radiated electric field becomes:

$$E_z^{sct} = \frac{j}{\omega 4\pi\varepsilon_0}k_0^2\int_{h-\frac{L}{2}}^{h+\frac{L}{2}} I(z')g(z,z')dz' \quad (2)$$

Inserting the relation for total Green function yields:

$$E_z^{sct} = \frac{1}{j\omega 4\pi\varepsilon_0}\int_{h-\frac{L}{2}}^{h+\frac{L}{2}} I(z')[g_0(z,z') + R_{TM}^F g_i(z,z')]dz' = \frac{1}{j\omega 4\pi\varepsilon_0}\int_{h-\frac{L}{2}}^{h+\frac{L}{2}} I(z')\left[\frac{e^{-jk_0R_0}}{r} + R_{TM}^F\frac{e^{-jk_0R_1}}{\mathrm{r1}}\right]dz' \quad (3)$$

where R_0 and R_1 according to Fig. 1 represent the distance from the source to the observation point:

$$R_0 = r - h\cos(\theta) \quad (4)$$
$$R_1 = r_1 + h\cos(\theta_1) \quad (5)$$

While r and r_1 represent distances from the center of the antenna to the observation point:

$$r = \sqrt{x^2 + y^2 + (h-z)^2} \quad (6)$$
$$r_1 = \sqrt{x^2 + y^2 + (h+z)^2} \quad (7)$$

In this manner, distance to the observation point is kept constant thus simplifying the integration process, while at the same time phase shift is taken into account rigorously.

Integrating expression (3) with the assumption of a triangular current distribution and Fresnel reflection coefficient yields an simple expression for the total electric field at the observation point:

$$E_z^{sctT} = \frac{1}{j\omega 4\pi\varepsilon_0}[(T_{11} + T_{12}) + R_{TM}^F(T_{21} + T_{22})] \quad (8)$$

where $T_{11}, T_{12}, T_{21} + T_{22}$ are exponential functions of h, L, $\cos(\theta)$, and $\cos(\theta_1)$:

$$T_{11} = -\frac{2I_0}{rLk_0^2\cos^2(\theta)}e^{-jk[r-h\cos(\theta)]} \cdot \left\{e^{-jk[(h+\frac{L}{2})\cos(\theta)]} + e^{-jk[(h-\frac{L}{2})\cos(\theta)]}\right\} \quad (9)$$

$$T_{12} = \frac{4I_0}{rLk_0^2\cos^2(\theta)}e^{-jk[r-h\cos(\theta)]}e^{-jk[h\cos(\theta)]} \quad (10)$$

$$T_{21} = -\frac{2I_0}{r_1Lk_0^2\cos^2(\theta_1)}e^{-jk[r_1+h\cos(\theta_1)]} \cdot \left\{e^{jk[(h+\frac{L}{2})\cos(\theta_1)]} + e^{jk[(h-\frac{L}{2})\cos(\theta_1)]}\right\} \quad (11)$$

$$T_{22} = \frac{4I_0}{r_11Lk_0^2\cos^2(\theta_1)}e^{-jk[r_1+h\cos(\theta_1)]}e^{jk[h\cos(\theta_1)]} \quad (12)$$

In a similar way, a simple expression for the total electric field at the observation point with the assumption of a sinusoidal current distribution and Fresnel reflection coefficient is obtained:

$$E_z^{sctS} = \frac{1}{j\omega 4\pi\varepsilon_0\sin\frac{k_0L}{2}}[(S_{11}+S_{12}+S_{13}+S_{14}) + R_{TM}^F(S_{21}+S_{22}+S_{23}+S_{24})] \quad (13)$$

where $S_{11}, S_{12}, S_{13}, S_{14}, S_{21}, S_{22}, S_{23}, S_{24}$ are exponential functions of h, L, $\cos(\theta)$, and $\cos(\theta_1)$:

$$S_{11} = \frac{I_0}{2rk(\cos(\theta)+1)}e^{-jk[r-h\cos(\theta)]}$$

$$\left\{e^{-jk[(h+\frac{L}{2})\cos(\theta)]} + e^{-jk[(h-\frac{L}{2})\cos(\theta)]}\right\} \quad (14)$$

$$S_{12} = -\frac{I_0\cos(\frac{k_0L}{2})}{2rk(\cos(\theta)+1)} e^{-jk[r-h\cos(\theta)]} e^{-jk[h\cos(\theta)]} \quad (15)$$

$$S_{13} = \frac{I_0}{2rk(-\cos(\theta)+1)} e^{-jk[r-h\cos(\theta)]} \quad (16)$$

$$\left\{e^{-jk[(h+\frac{L}{2})\cos(\theta)]} + e^{-jk[(h-\frac{L}{2})\cos(\theta)]}\right\}$$

$$S_{14} = -\frac{I_0\cos(\frac{k_0L}{2})}{2rk(-\cos(\theta)+1)} e^{-jk[r-h\cos(\theta)]} e^{-jk[h\cos(\theta)]} \quad (17)$$

$$S_{21} = \frac{I_0}{2r_1k(\cos(\theta_1)+1)} e^{-jk[r_1+h\cos(\theta_1)]}$$

$$\left\{e^{jk[(h+\frac{L}{2})\cos(\theta_1)]} + e^{jk[(h-\frac{L}{2})\cos(\theta_1)]}\right\} \quad (18)$$

$$S_{22} = -\frac{I_0\cos(\frac{k_0L}{2})}{2r_1k(\cos(\theta_1)+1)} e^{-jk[r_1+h\cos(\theta_1)]} e^{jk[h\cos(\theta_1)]} \quad (19)$$

$$S_{23} = \frac{I_0}{2r_1k(-\cos(\theta_1)+1)} e^{-jk[r_1+h\cos(\theta_1)]}$$

$$\left\{e^{jk[(h+\frac{L}{2})\cos(\theta_1)]} + e^{jk[(h-\frac{L}{2})\cos(\theta_1)]}\right\} \quad (20)$$

$$S_{24} = -\frac{I_0\cos(\frac{k_0L}{2})}{2r_1k(-\cos(\theta_1)+1)} e^{-jk[r_1+h\cos(\theta_1)]} e^{jk[h\cos(\theta_1)]}$$

(21)

APPENDIX B

Whole body averaged SAR for cylindrical body model:

$$SAR_{WB} = \frac{1}{V}\int_V SAR dV \quad (1)$$

where

$$SAR_{WB} = \frac{\sigma k^2}{4\rho La^4\pi^3(\sigma^2+\omega^2\varepsilon^2)} \frac{1}{|J_1(j^{-1/2}ka)|^2} \int_0^a |J_0(j^{-1/2}k\zeta|^2 d\zeta \int_0^L |I_z(z)|^2 dz \quad (2)$$

$$\frac{\sigma k^2}{4\rho La^4\pi^3(\sigma^2+\omega^2\varepsilon^2)} \frac{1}{|J_1(j^{-1/2}ka)|^2} = C \quad (3)$$

$$\int_0^a |J_0(j^{-1/2}k\zeta|^2 d\zeta = I_1 \quad (4)$$

$$\int_0^L |I_z(z)|^2 dz = I_2 \quad (5)$$

$$SAR_{WB} = CI_1I_2 \quad (6)$$

Since current distribution in cylindrical human body model depends of Bessel function, axial current should have a form similar to (7), where:

$$I(z) = C_1 cos\gamma z + C_2 sin\gamma z \quad (7)$$

$$\gamma^2 = k^2(1 - \frac{j4\pi Z_c(\zeta)}{kZ_c\Psi_{dR}}) \quad (8)$$

where k is the free space wave number, Z_c=120π is the free space impedance and $Z_c(\zeta)$ is the HF region, the impedance per unit length is given by

$$k = \omega\sqrt{\mu_0\varepsilon_0} \quad (9)$$

$$Z_c(\zeta) = \frac{k}{2a\pi\sigma}\frac{J_0(j^{-1/2}k\zeta)}{J_1(j^{-1/2}ka)} \quad (10)$$

$$\Psi_{dR} = csc\gamma(h-|z|)\int_{-h}^{h} sin\gamma(h-|z'|)\left[\frac{coskR}{R} - \frac{coskR_h}{R_h}\right]dz' \quad (11)$$

Enida Cero Dinarević was born in Konjic on March 29, 1990. She studied at the University of Sarajevo, and got Bachelor degree (2008-2011) and Master degree (2011-2013) in Electrical Engineering at Department for Telecommunication. Her employment experience included the American University in Sarajevo, Codding Giants School for programing, and BH Telecom. Her special fields of interest include EMC.

Dragan Poljak (SM' 13) received his PhD in el. Eng. in 1996 from the Univ. of Split, Croatia. He is the Full Prof. at Dept. of Electron. and Computing, Univ. of Split. His research interests are oriented to computational electromagnetics (electromagn. compatibility, bioelectromagnetics and plasma physics). To date Prof. Poljak has published more than 160 journ. and 250 conf. papers, and authored some books, e.g. two by Wiley, New Jersey and one by Elsevier, St Louis. He is a Senior member of IEEE, a member of Editorial Board of Eng. Anal. with Boundary Elements, Math. Problems in Eng. And IET Sci. Measur. & Techn. He was awarded by several prizes for his achievements, such as National Prize for Science (2004), Croatian sect. of IEEE annual Award (2016), Technical Achievement Award of the IEEE EMC Society (2019) and George Green Medal from University of Mississippi (2021). From May 2013 to June 2021 Prof. Poljak was a member of the board of the Croatian Science Foundation. He is currently involved in ITER physics EUROfusion collab. and in Croatian center for excellence in research for tech. sciences. He is active in few Working Groups of IEEE/Internat. Committee on Electromagnetic Safety (ICES) Tech. Comm. 95 SC6 EMF Dosimetry Modeling.

Vicko Dorić was born on 27th of April 1974. in Split, Croatia. He received the P.hd. degree from the University of Split, Split, Croatia, in 2009. He is currently Assistant Professor at the Department of Electronics and Computing at the University of Split, Faculty of Electrical Engineering, Mechanical Engineering and Naval Architecture (FESB). Vicko Doric is a member of IEEE since 2005. He served as a President of Croatian chapter of IEEE EMC society for the period from 2016. to 2019. His research interests include computational methods in electromagnetics, particularly in the numerical modeling of wire antenna structures with strong applications in the field of electromagnetic compatibility. To date, he has published two books, 18 journal papers and 73 conference papers in the area of computational electromagnetics and electromagnetic compatibility.